

CHEMISTRY

AN **ASIAN** JOURNAL

www.chemasianj.org

Accepted Article

Title: C-H Direct Arylated 6H-Indolo[2,3-b]quinoxaline Derivative as Thickness-Dependent Hole Injection Layer

Authors: Dai Dong, Da Fang, Hairong Li, Caixia Zhu, Xianghua Zhao, Jiewei Li, Lingzhi Jin, Linghai Xie, Lin Chen, Jianfeng Zhao, Hongmei Zhang, and Wei HUANG

This manuscript has been accepted after peer review and appears as an Accepted Article online prior to editing, proofing, and formal publication of the final Version of Record (VoR). This work is currently citable by using the Digital Object Identifier (DOI) given below. The VoR will be published online in Early View as soon as possible and may be different to this Accepted Article as a result of editing. Readers should obtain the VoR from the journal website shown below when it is published to ensure accuracy of information. The authors are responsible for the content of this Accepted Article.

To be cited as: *Chem. Asian J.* 10.1002/asia.201700112

Link to VoR: <http://dx.doi.org/10.1002/asia.201700112>

A Journal of



A sister journal of *Angewandte Chemie*
and *Chemistry – A European Journal*

WILEY-VCH

C-H Direct Arylated 6*H*-Indolo[2,3-*b*]quinoxaline Derivative as Thickness-Dependent Hole Injection Layer

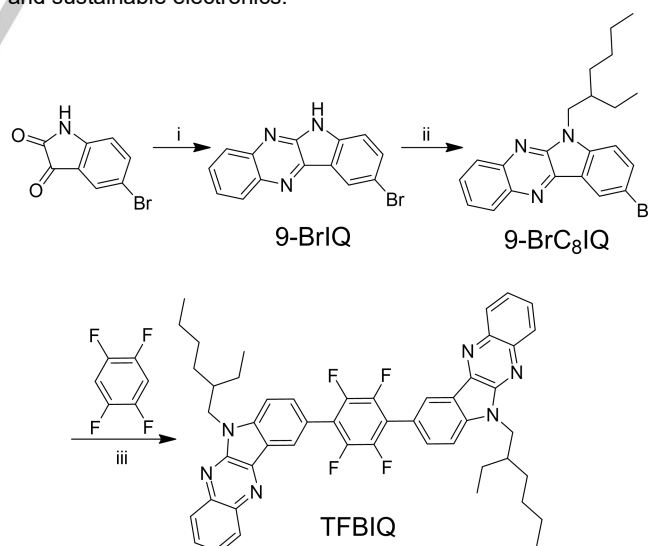
Dai Dong,^a Da Fang,^b Hairong Li,^a Caixia Zhu,^a Xianghua Zhao,^c Jiwei Li,^a Lingzhi Jin,^b Linghai Xie,^b Lin Chen,^d Jianfeng Zhao,^{*a,b} Hongmei Zhang,^{*b} Wei Huang^{*a,b}

Abstract: A novel perfluoro-1,4-phenylene 6*H*-indolo[2,3-*b*]quinoxaline derivative (**TFBIQ**) was designed and synthesized using a C-H direct arylation method. The optoelectrical properties of the obtained **TFBIQ** were fully characterized by ultraviolet-visible spectroscopy, photoluminescence spectroscopy, cyclic voltammetry, and a group of Alq₃-based green organic light-emitting diodes (OLEDs). Device A using 0.5 nm-thick **TFBIQ** as the interfacial modification layer exhibits the best five advantages of device performance including the lowest minimum turn-on voltage as low as 3.1 V, the maximum luminescence intensity as high as 26564 cd m⁻², the highest current density value as 348.9 mA cm⁻² at the voltage of 11 V, the smallest efficiency rolling-off, as well as the biggest power efficiency as 1.46 lm W⁻¹ prior to all of other devices with thicker **TFBIQ** and also 10 nm-thick MoO₃ as hole injection layers (HIL). As a promising candidate as organic HIL material, the as-prepared **TFBIQ** exhibits a strong thickness effect on the performance of corresponding OLEDs. Besides, the theoretical calculated vertical ionization potential of the fluorinated **TFBIQ** presents a clue for a better anti-oxidation stability than that of the non-fluorinated structure.

Introduction

During the past decades, organic light-emitting diodes (OLEDs) have attracted an enormous research engagement because of their prosper applications in the fields of solid-state lighting and flexible optoelectronic displays.¹⁻⁴ In order to increase the illuminated efficiency of emitting devices, great improvements have been achieved including optimizing device structures, exploring novel emitting materials⁵⁻⁸ and adjusting the carrier buffer ability⁹ by enhancing the transport of electron than

hole between the active layers.^{10, 11} Especially, the electron-hole balance between the active layers determines the specific performance of the sandwiched-like light-emitting device. It has been proved that the modification of the electrode/organic interface could exert influence on the carrier injection to improve the device performance.¹²⁻¹⁴ Therefore, it is significant to develop suitable HIL materials inserted between the hole transport layer and the transparent anode to optimize the charge injection and transport balance.¹⁵⁻¹⁷ Up to now, a few but insufficient organic HIL materials including 2-TNATA, m-MTDATA,¹⁸ CuPc,¹⁹ and PEDOT:PSS¹² have been developed to compete with the non-renewable inorganic HIL materials.²⁰⁻²³ In this situation, it is emergent to discover more novel, low cost, eco-friendly, and large-scale preparative organic HIL materials. However, there are few reports about the application of 6*H*-indolo[2,3-*b*]quinoxaline derivatives (**IQs**) as the HIL material. Since the discovery,²⁴ **IQs** have not only many significant applications in biochemistry and medicinal chemistry²⁵⁻²⁹ but also in recent material science as electron transport and light-emitting layers of organic electronic devices³⁰⁻³⁵ due to their unique π -conjugated structures and exceptional stabilities. Although the synthetic methods and mechanisms have been systematically studied,^{36, 38} the related C-C coupling methods are usually not eco-friendly^{32, 35} due to the more toxic organic tin reagents or harsh organic lithium reagents than C-H direct arylation.^{39, 40} Therefore, the competitive research and development of eco-friendly organic HIL materials represent an effective strategy for green and sustainable electronics.^{41, 42}



Scheme 1. The synthetic routine of **TFBIQ**, i) *o*-phenylenediamine, HOAc, 120 °C, N₂, over night; ii) 3-(bromomethyl)heptane, tetrabutyl ammonium bromide, K₂CO₃, DMF, 140 °C, 5h; iii) Pd(OAc)₂, P(*t*-Bu)₂Me-HBF₄, K₂CO₃, *N,N*-dimethyl acetamide, 150 °C, N₂, 10h.

- [a] D. Dong, H. Li, C. Zhu, J. Li, J. Zhao, W. Huang
Key Laboratory of Flexible Electronics (KLOFE) & Institute of Advanced Materials (IAM), Jiangsu National Synergetic Innovation Center for Advanced Materials (SICAM)
Nanjing Tech University (NanjingTech), 30 South Puzhu Road, Nanjing 211816, P.R. China
E-mail: iamwhuang@njtech.edu.cn
- [b] D. Fang, L. Jin, L. Xie, H. Zhang
Key Laboratory for Organic Electronics & Information Displays (KLOEID) and Institute of Advanced Materials, Nanjing University of Posts & Telecommunications, Nanjing 210023, P.R. China
E-mail: iamhmzhang@njupt.edu.cn
- [c] X. Zhao
College of Chemistry and Chemical Engineering, Xinyang Normal University, Xinyang 464000, Henan, China
- [d] L. Chen
Nanjing Polytechnic Institute
Nanjing 210048
P.R. China

Supporting information for this article is given via a link at the end of the document.

In this work, we reported a novel hole injection layer material based on IQ derivative entitled 9,9'-(perfluoro-1,4-phenylene)bis(6-(2-ethylhexyl)-6*H*-indolo[2,3-*b*]quinoxaline) (**TFBIQ**) presented in Scheme 1. The molecule structure of **TFBIQ** contains two IQ moieties and a bridged perfluoro-1,4-phenylene group jointed by a facile C-H direct arylation.^{41, 43-46} Symmetrical tetrafluoro-substituted phenylene would promisingly endow **TFBIQ** with low vertical ionization potential (IP_v) leading to its anti-oxidation property (Table S1). The optoelectrical properties, film morphologies, and thermal properties of **TFBIQ** were measured by UV-visible (UV-vis), photoluminescence (PL) spectra, cyclic voltammetry (CV), atomic force microscopy (AFM), thermo-gravimetric analysis (TGA), and differential scanning calorimetry (DSC) analysis. We also fabricated several green OLEDs to verify the usability test of **TFBIQ** as the HIL.

Results and Discussion

Synthesis. The synthesis of the IQ derivatives were accomplished as illustrated in Scheme 1. **9-BrIQ** was prepared by the acid catalyzed cyclocondensation⁴⁷⁻⁴⁹ from bromoisatin and *o*-phenylenediamine as a yellow precipitate in 84% yield which was directly used for the next step without further purification. **9-BrC₈IQ** was obtained via a *N*-alkylation reaction from **IQ** and 3-(bromomethyl)heptane in the presence of K₂CO₃ in DMF with a yield of 50%. The target molecule **TFBIQ** was obtained through the C-H direct arylation from **9-BrC₈IQ** and 1,2,4,5-tetrafluorobenzene using Pd(OAc)₂ as the catalyst in 45% yield avoided the reported toxic and harsh condition. The obtained chemicals were confirmed by ¹H-NMR spectroscopy and MALDI-TOF mass spectroscopy in good agreement with the molecular structures presented in Scheme 1.

Photophysical properties. As presented in Figure 1 and Table 1, the photophysical behaviors of **TFBIQ** have been examined by measuring absorption and fluorescence spectra in chloroform solution with a concentration of 1.0×10^{-5} mol L⁻¹ and solid film. **TFBIQ** in solution exhibited two absorption bands at 360 nm and 410 nm. The optical energy gap was calculated as 2.75 eV in solution. There was about 4 nm redshift for **TFBIQ** from 471 nm in solution to 475 nm in solid film indicating the existence of a rigid π -conjugation. Cyclic voltammetry (CV) (Figure 2b) was measured to estimate highest occupied molecular orbital (HOMO) and lowest unoccupied molecular orbital (LUMO). HOMO value was calculated to be -5.96 eV from the oxidation potential according to the empirical equation $\text{HOMO} = -[4.4 + E_{\text{ox}}]$.⁵⁰ The LUMO value was subsequently calculated to be -3.21 eV according to the optical energy gap measured from the optical edge listed in Table 1. The HOMO level of **TFBIQ** is lower than the reported value of *N*⁴,*N*^{4'}-di(naphthalen-1-yl)-*N*⁴,*N*^{4'}-diphenyl-[1,1'-biphenyl]-4,4'-diamine (NPB) and work function of indium tin oxide (ITO)⁵¹ hinting the potential use as the HIL in OLEDs.

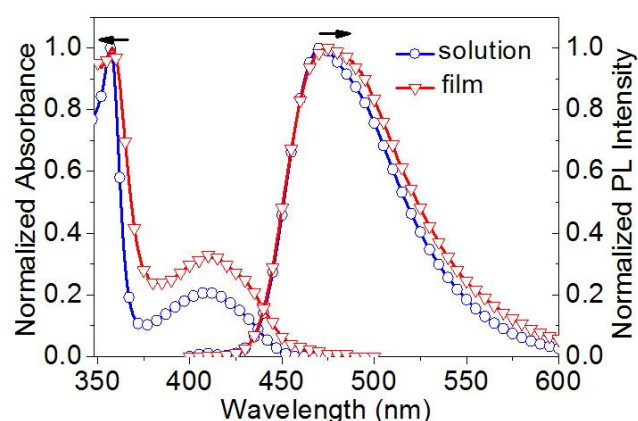


Figure 1. UV-vis and PL spectra in chloroform (1.0×10^{-5} mol L⁻¹) and in thin film of **TFBIQ**.

Table 1. Physical and thermal properties of **TFBIQ**.

Materials	λ_{abs} [nm]	$\lambda_{\text{max,em}}$ [nm]	HOMO/ LUMO[eV]	Gap _{opt} [eV]	T _g /T _d [°C]
TFBIQ	357, 408	471	5.96 / 3.21	2.75	N.D./411

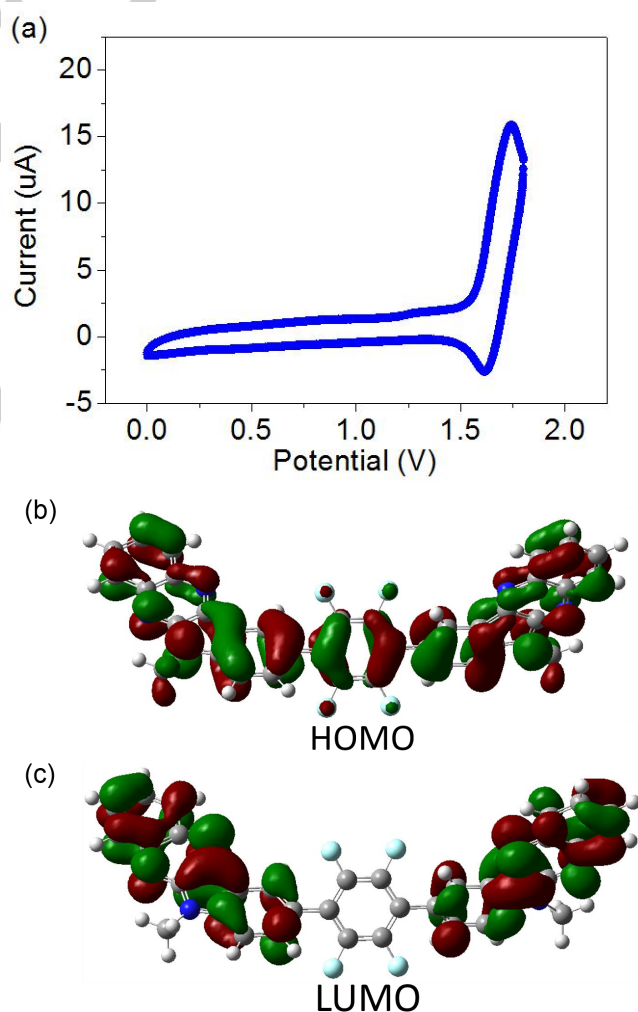
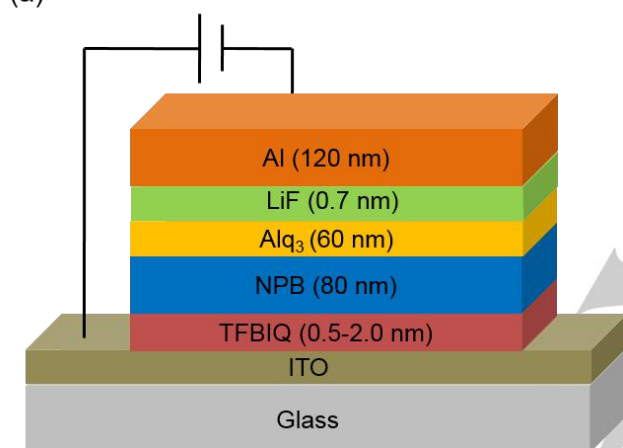


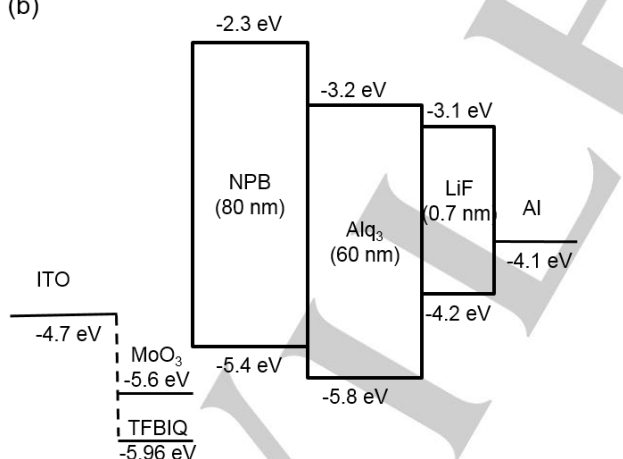
Figure 2. (a) Cyclic voltammogram recorded for **TFBIQ** in dichloromethane; (b, c) Wave functions for the HOMO and LUMO of **TFBIQ** molecule.

The DFT calculation was performed to understand the electronic structure of **TFBIQ** as shown in Figure 2b and 2c. The HOMO delocalizes over the whole conjugated backbone including indole, quinoxaline and perfluoro-1,4-phenylene. LUMO just localizes on two quinoxaline moieties. The vertical ionization potential (IP_v) for the fluorinated **TFBIQ** is -7.38 eV (Table S1) which is high enough to prevent **TFBIQ** from the oxidation. Besides, the IP_v of **TFBIQ** is higher than the non-fluorinated **BIQ** which hints **TFBIQ** could potentially adjust and buffer the hole-injection behavior. The hole reorganization energy of **TFBIQ** is 0.50 eV lower than 0.57 eV of **BIQ** indicating a smaller energy loss for the hole transfer. Both of the two properties suggest that fluorinated **TFBIQ** is much more suitable for HIL material than non-fluorinated **BIQ**. **TFBIQ** also exhibits good thermal stability with a very high decomposition temperature (*T_d*) due to the high molecular weight and the rigid backbone. The value corresponding to 5% weight loss was 411°C for **TFBIQ** (Table 1, Figure S5, S6).

(a)



(b)



(c)

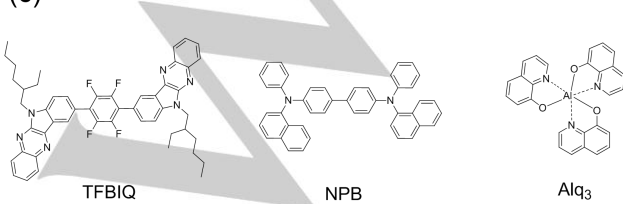


Figure 3. (a) Schematic configuration of the OLEDs; (b) Energy band diagrams of the OLEDs; (c) molecule structures of organic materials.

Table 2. The structures of the OLEDs showing the different layer thickness of **TFBIQ**-HIL and MoO₃ used in the devices.

Devices	Structures
A	ITO/ TFBIQ (0.5 nm)/NPB (80 nm)/Alq ₃ (60 nm)/LiF (0.7 nm)/Al (120 nm)
B	ITO/ TFBIQ (1 nm)/NPB (80 nm)/Alq ₃ (60 nm)/LiF (0.7 nm)/Al (120 nm)
C	ITO/ TFBIQ (1.5 nm)/NPB (80 nm)/Alq ₃ (60 nm)/LiF (0.7 nm)/Al (120 nm)
D	ITO/ TFBIQ (2 nm)/NPB (80 nm)/Alq ₃ (60 nm)/LiF (0.7 nm)/Al (120 nm)
X	ITO/MoO ₃ (10 nm)/NPB (80 nm)/Alq ₃ (60 nm)/LiF (0.7 nm)/Al (120 nm)

Electroluminescent (EL) performance. In order to evaluate the ability of **TFBIQ** to adjust the electron/hole injection and the transport balance, five OLED devices were fabricated using **TFBIQ** or MoO₃ as the HIL materials with thickness from 0.5, 1, 1.5 to 2 nm (Device A, B, C, and D) for the former and 10 nm (Device X) for the latter, respectively. Their EL characteristics were measured using a general device configuration of ITO/**TFBIQ** or MoO₃/NPB (80 nm)/Alq₃ (60 nm)/LiF (0.7 nm)/Al (120 nm) as shown in Figure 3a. Their device structures and corresponding characteristics were listed in Table 2 and Table 3. For comparison, the only difference between these devices is the alternative HIL materials with different thickness.

Table 3. The summary of OLEDs characteristics.

Device	V _{on} (V) ^{a)}	L _{max} ^{b)} (cd m ⁻²)	LE _{max} ^{b)} (cd A ⁻¹)	PE _{max} ^{b)} (lm W ⁻¹)	EQE _{max} ^{c)}	CIE (x, y) ^{d)}
A/0.5nm	3.1	26564	4.10	1.46	1.36	0.30,0.55
B/1nm	3.5	22451	4.21	1.29	1.45	0.30,0.55
C/1.5nm	4.9	20008	4.10	1.09	1.58	0.30,0.55
D/2nm	6.5	19768	4.05	0.95	1.41	0.31,0.54
X/10 nm	3.1	22183	5.04	2.12	-	0.30,0.55

^{a)} V_{on}, Turn-on voltages at 1 cd m⁻²; ^{b)} L_{max}, maximum luminance; PE_{max}, maximum power efficiency; LE_{max}, maximum luminance efficiency; ^{c)} EQE_{max}, maximum external quantum efficiency; ^{d)} CIE coordinates were recorded at 10 V for devices A-D.

Figure 4 presents the current density–voltage–luminance (J–V–L), and luminance efficiency–luminance (LE–L) characteristics with the main parameters tabulated in Table 3. As shown in the J–V–L graph and parameters in Table 3, device A and B using 0.5 nm- and 1 nm-thick **TFBIQ** as the interfacial modification layer exhibit a good minimum turn-on voltage (V_{on}), as low as 3.1 V and 3.5 V at 1 cd m⁻². These two values are almost the same as 3.1 V which is the same as the V_{on} value of device X with 10 nm-thick MoO₃, respectively. Especially, the maximum luminescence intensity (Figure 4a, rightwards arrows) reaches as high as 26564 cd m⁻² of device A surpassing over 22451 cd m⁻² of device B and also 22183 cd m⁻² of device X with MoO₃ as the HIL. Besides, at the voltage of 11 V, the current density (J) (Figure 4a, leftwards arrows) of devices A-D were 348.9 mA cm⁻², 137.7 mA cm⁻², 21.1 mA cm⁻², 5.4 mA cm⁻², respectively. It is obvious that device A exhibits the best J which is 2.1 times than the corresponding value as 167.7 mA cm⁻² of device X. When the thickness of **TFBIQ** increased to 1.5 nm and

2 nm, the V_{on} values of device C and D reach as high as 4.9 V and 6.5 V. It is indicated that these turn-on voltages of **TFBIQ** HIL based OLEDs have strong dependence on the HIL thickness. Meanwhile, the corresponding maximum luminance efficiencies (LE) measured on devices A-D were rather close as high as 4.10 cd A^{-1} , 4.21 cd A^{-1} , 4.10 cd A^{-1} , and 4.05 cd A^{-1} , respectively, reaching 4/5 of the LE_{max} value as 5.04 cd A^{-1} of device X (Figure 4b, Table 3).

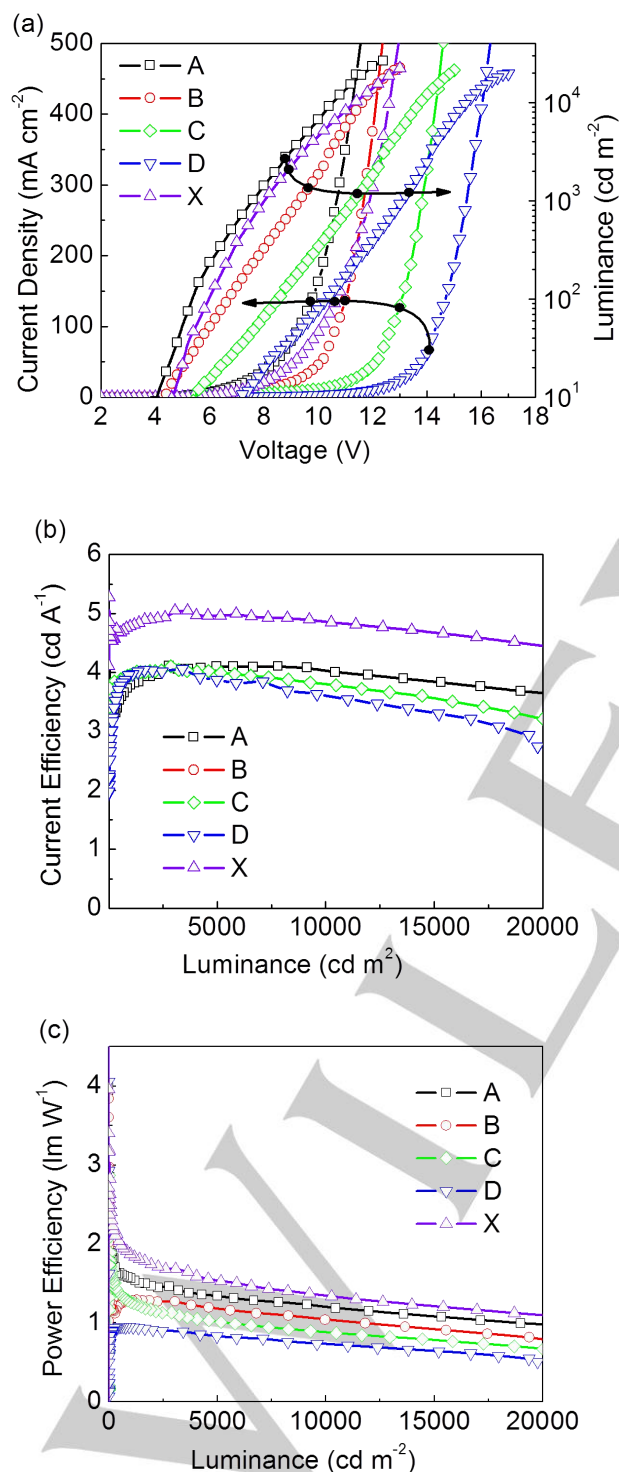


Figure 4. The (a) J-V-L characteristics of devices A-D, X; (b) luminance efficiency-luminance characteristics of devices A-D, X; (c) power efficiency-luminance characteristics of devices A-D, X.

As shown in Figure 4b and Table 3, it is found that devices A-D with the thinner **TFBIQ** as the HIL exhibited better device stability with reduced efficiency rolling-off. At the same luminance intensity of 19000 cd m^{-2} , there were 89.3%, 78.3%, 80.2%, and 73.3% efficiency rolling-off while the LE of **TFBIQ** in devices A-D reaching 3.66, 3.30, 3.29 and 2.97 cd A^{-1} compared to their LE_{max} , respectively. Among them, Device A presented the best device stability quite close to 89.2% efficiency rolling-off of device X when its LE arrived at 4.50 cd A^{-1} divided by its LE_{max} (5.04 cd A^{-1}). As shown in Figure 4c, device A exhibited the best performance of PE_{max} as 1.46 lm W^{-1} larger than the values from 1.29, 1.09 to 0.95 lm W^{-1} of device B, C, and D presenting a gradually reasonable rolling-off. However, the external quantum efficiency (EQE) of device A reached 1.36% which is lower than that of other three device B, C and D with higher EQE as 1.45%, 1.58%, and 1.41%, respectively.

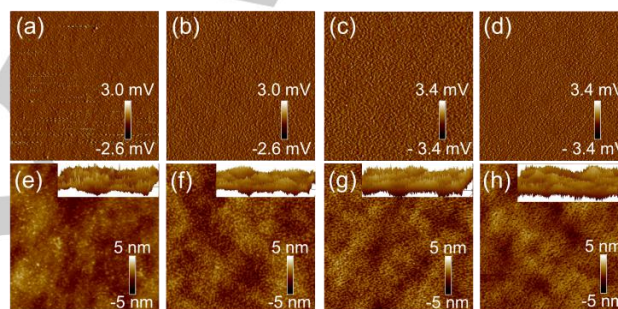


Figure 5. AFM topographic (a-d), height (e-h), and inset roughness images of vapor deposited **TFBIQ** on Si substrates with four different thickness: 0.5 nm (a, e), 1 nm (b, f), 1.5 nm (c, g), and 2 nm (d, h).

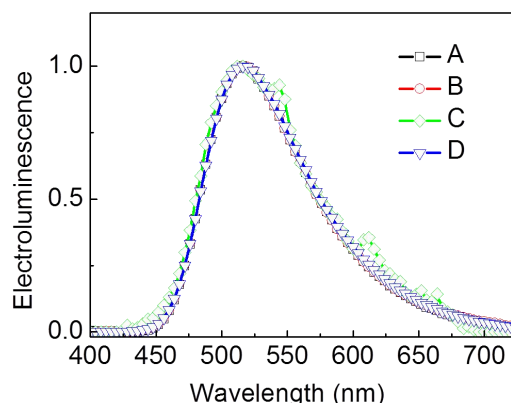


Figure 6. EL spectra of devices A-D at 9 V.

The operating voltage exhibited an obvious growth trend while the LE and PE values show a decreasing tendency. It is indicated that the optimized thickness of 0.5 nm was the most suitable physical parameter leading to the best electroluminescent performance of hole injective **TFBIQ**-based devices. It should be noted that the similar but lower HOMO

levels -5.96 eV of **TFBIQ** than -5.4 eV of NPB leading to the enhanced hole balance and transfer from **TFBIQ**-modified ITO to higher energy stated NPB layer. Meanwhile, the quite close HOMO level of **TFBIQ** to that of MoO₃ (-5.6 eV)⁵¹ suggests a reasonable explanation for the comparative performance (Table 3) of **TFBIQ**-based OLED devices.

Figure 5 presents the AFM 5 $\mu\text{m} \times 5 \mu\text{m}$ topographic images (5a-d) and phase images (5e-g) of the vapor deposited **TFBIQ** films with the thickness from 0.5 nm, 1 nm, 1.5 nm to 2 nm on bare Si substrates under vacuum with quite similar roughness and gradually increased thickness shown by the inset images. All the surface morphologies are determined as quite similar smoothing patterns without remarkable grain domains which are favorable for the homogeneous interface modification of ITO electrode. The modified interface impedes the lateral **TFBIQ** molecular diffusion and suppresses the **TFBIQ** molecular crystallization implying the degradation of device stability. Figure 6 shows the EL spectra of devices A-D driven at 9 V. It is clearly seen that the Alq₃ green light emission (peaking at ~515 nm) can be observed in all devices.

Conclusions

In summary, a fluorinated 6*H*-indolo[2,3-*b*]quinoxaline derivative **TFBIQ** synthesized via the palladium-catalyzed C-H direct arylation was successfully used as the HIL in Alq₃ based green electroluminescent devices. When the thickness ranges from 0.5 nm to 1 nm, device A with 0.5 nm-thick **TFBIQ** as the HIL exhibits the best device performance, especially, in the four aspects of V_{on} , L_{max} , J and the lowest efficiency rolling-off close to that of device X with MoO₃ as the HIL. These results reveal that **TFBIQ** would be a pioneer **IQ**-based molecule for a new series of highly performed HIL materials suitable for green and sustainable organic light-emitting diodes.

Experimental Section

Materials. 5-Bromoisatin, 3-(bromomethyl)heptane, tetra(*n*-butyl)ammonium bromide (TBAB), Pd(OAc)₂, 1,2,4,5-tetrafluorobenzene and P(*t*-Bu)₂Me-HBF₄ were purchased from Nanjing Fountain Global Displays and ENERGY CHEMICAL. Other reagents and solvents were purchased from Sinopharm Chemical Reagent Co., Ltd. All solvents were used without further purification.

Synthesis of 9-bromo-6*H*-indolo[2,3-*b*]quinoxaline (9-BrIQ). A mixture of 5-bromoisatin (2.26 g, 10 mmol), benzene-1,2-diamine (1.62 g, 15 mmol) and acetic acid (60 ml) under nitrogen atmosphere was heated at 80 °C and stirred over night. After cooling to room temperature, the reaction mixture was filtered, dried in vacuum oven and gave a yellow solid 2.43 g with a yield of 84%. The solid was directly used for the next step.

Synthesis of 9-bromo-6-(2-ethylhexyl)-6*H*-indolo[2,3-*b*]quinoxaline (9-BrC₈IQ). 9-BrIQ (2.98 g, 10 mmol), 3-(bromomethyl)heptane (3.10 g, 15 mmol), and TBAB (0.32 g, 1 mmol) were dissolved with 20 ml of DMF in a 100 ml round-bottom flask. K₂CO₃ (4.14 g, 30 mmol) was then added to the solution. The mixture was stirred at 140 °C for 5 h. After cooling to ambient temperature the solution was poured into saturated NaCl solution, stirred for 30 min, and then extracted with dichloromethane. The combined organic layer was dried over anhydrous MgSO₄, filter and

evaporated to dryness. The residue was purified by silica gel column chromatography using petroleum ether/ethyl acetate mixed solvent as eluent. A yellow solid as **9-BrC₈IQ** with a yield of 50% was obtained after drying in vacuum oven. ¹H NMR (400 MHz, CDCl₃) δ 8.61 (s, 1H), 8.29 (d, J = 8.4 Hz, 1H), 8.13 (d, J = 8.4 Hz, 1H), 7.77 (t, J = 8.5 Hz, 2H), 7.69 (t, J = 8.3 Hz, 1H), 7.35 (d, J = 8.6 Hz, 1H), 4.35 (d, J = 7.5 Hz, 2H), 2.15 (m, 1H), 1.51 – 1.27 (m, 6H), 1.25 (m, 2H), 0.94 (t, J = 7.5 Hz, 3H), 0.85 (t, J = 7.2 Hz, 3H); ¹³C NMR (100 MHz, CDCl₃) δ 145.90, 143.14, 140.89, 139.38, 138.39, 133.19, 129.38, 128.96, 127.98, 126.09, 125.26, 121.07, 113.44, 111.09, 45.53, 38.49, 30.66, 28.48, 24.11, 22.92, 13.95, 10.63. GC-MS calculated for C₂₂H₂₄BrN₃, 410.35; found 410.9.

Synthesis of 9,9'-(perfluoro-1,4-phenylene)bis(6-(2-ethylhexyl)-6*H*-indolo[2,3-*b*] quinoxaline) (TFBIQ). A 50 ml round-bottom flask containing a magnetic stirring bar was flame-dried under vacuum and filled with nitrogen after cooling to room temperature. **9-BrC₈IQ** (410 mg 1 mmol), K₂CO₃ (345 mg, 2.5 mmol), Pd(OAc)₂ (11 mg, 0.05 mmol), and P(*t*-Bu)₂Me-HBF₄ (25 mg, 0.1 mmol) were added to this vessel. The flask was evacuated and backfilled with nitrogen for 3 times. Then, 1,2,4,5-tetrafluorobenzene (120 mg, 0.8 mmol) and the solvent *N,N*-dimethylacetamide (10 ml) were added with stirring at room temperature for several minutes. The flask was then placed into oil bath, heated to 150 °C and refluxed overnight. After cooling to room temperature, the reaction mixture was poured into saturated NaCl solution, stirred for 1 h and then extracted with dichloromethane. The organic layer was dried over anhydrous Na₂SO₄, filtered and evaporated to dryness. The crude product was purified by flash column chromatography using petroleum ether/ethyl acetate mixed solvent as eluent, to afford a desired product **TFBIQ** after drying in vacuum oven, 182 mg, yield 45%. ¹H NMR (400 MHz, CDCl₃) δ 8.74 (s, 2H), 8.35 (d, J = 8.4 Hz, 2H), 8.17 (d, J = 8.5 Hz, 2H), 7.90 (d, J = 8.4 Hz, 2H), 7.80 (t, J = 8.4 Hz, 2H), 7.72 (t, J = 8.2 Hz, 2H), 7.64 (d, J = 8.2 Hz, 2H), 4.45 (d, J = 7.5 Hz, 4H), 2.30-2.20 (m, 2H), 1.46 (m, 12H), 1.29 (m, 4H), 1.00 (t, J = 7.4 Hz, 6H), 0.89 (t, J = 7.2 Hz, 6H); ¹³C NMR (100 MHz, CDCl₃) δ 146.34, 144.78, 140.86, 139.48 (d, J = 8.8 Hz), 132.58, 129.45, 128.90, 128.05, 126.16, 124.63, 119.82 (d, J = 9.4 Hz), 109.91, 45.65, 38.65, 30.74, 28.54, 24.19, 23.01, 14.01, 10.67. MALDI-TOF MS: calcd for C₅₀H₄₈F₄N₆ 808.95, found 811.74.

Methods. ¹H NMR and ¹³C NMR spectra were measured on a Bruker ARX 400 spectrometer. The UV-vis absorption and fluorescence spectra were recorded on a Shimadzu UV-1750 and Hitachi F-460C spectrophotometer, respectively. MS were collected on MALDI TOF2 AXIMA mass spectrometer. The glass transition temperatures of compounds were determined under a nitrogen atmosphere by DSC using a NETZSCH DSC214 Polyma instrument. The decomposition temperature corresponding to 5% weight loss was conducted on a METTLER TOLEDO TGA2 thermal analyzer. Density function theory (DFT) at the B3LYP/6-31G(d)⁵² level was implemented to optimize the geometry and calculate the electronic structure of the rigid **TFBIQ** molecular structure in Gaussian 09 software⁵³ to relax the structure fully.⁵⁴ Cyclic voltammetry experiment was carried out using a three-electrode system employing a glassy carbon electrode as the working electrode, a Ag/Ag⁺ electrode as the reference electrode, and a Pt wire as the counter electrode. The redox potentials were measured in dichloromethane, using 0.1 M *n*-Bu₄NPF₆ as the supporting electrolyte with a scan rate of 100 mV s⁻¹.

Electroluminescent tests. The commercial ITO-coated glass substrates with a sheet resistance of around 10 Ω/m^2 were used as the anode, which were successively rinsed with detergent, de-ionized water, acetone, and isopropyl alcohol in an ultrasonic bath for 15 min, respectively. The cleaned and dried ITO glass substrates were treated with oxygen plasma for 5 min. The **TFBIQ** was evaporated at 220 °C with four thickness from 0.5, 1, 1.5 to 2 nm. The OLEDs were prepared by thermal evaporation in a high-vacuum system with the pressure less than 5×10^{-4} Pa. **TFBIQ**, NPB, Alq₃, 0.7 nm LiF and 120 nm Al were evaporated onto ITO in turn. The evaporation rates were monitored by frequency counter, and calibrated by Dektak 6 M Profiler (Veeco). The overlap area between ITO

and Al electrodes was 16 mm² as the emissive size of devices. The devices have the same 80 nm NPB, 60 nm Alq₃, 0.7 nm LiF, and 120 nm Al. Figure 3 shows the energy level diagrams of the fabricated devices and the molecular structures of TFBQ, Alq₃ and NPB used in these devices. The current–voltage–brightness characteristics were measured by using a Keithley source measurement unit (Keithley 2400 and Keithley 2000) with a calibrated silicon photodiode. All devices were measured without encapsulation at room temperature.

Acknowledgements

We thank the 973 program (2015CB932200), the National Natural Science Foundation of China (NSFC, 21502091, 61274065, 21603104, 21003706), and the Natural Science Foundation of Jiangsu Province (BK20130912 and 14KJB430017) and Ministry of Education and Synergetic Innovation Center for Organic Electronics and Information Displays for financial support.

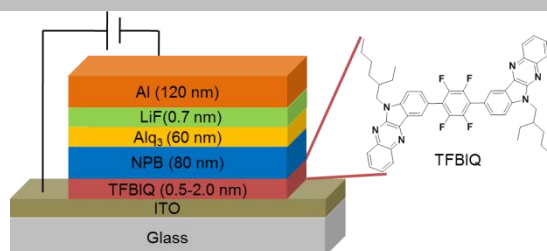
Keywords: C–H direct arylation • 6H-indolo[2,3-*b*]quinoxaline • hole injection layer • OLED •

References:

1. S. Reineke, F. Lindner, G. Schwartz, N. Seidler, K. Walzer, B. Lussem, K. Leo, *Nature* **2009**, *459*, 234–238.
2. T. L. Chiu, Y. P. Hsiao, Y. T. Chuang, C. M. Lai, H. C. Ho, *Org. Electron.* **2014**, *15*, 785–791.
3. T. Matsushima, C. Adachi, *Appl. Phys. Lett.* **2006**, *89*, 253506.
4. C. F. Qiu, H. Y. Chen, M. Wong, H. S. Kwok, *IEEE T. Electron Dev.* **2002**, *49*, 1540–1544.
5. M. K. Leung, Y. H. Hsieh, T. Y. Kuo, P. T. Chou, J. H. Lee, T. L. Chiu, H. J. Chen, *Org. Lett.* **2013**, *15*, 4694–4697.
6. C. C. Lee, M. K. Leung, P. Y. Lee, T. L. Chiu, J. H. Lee, C. Liu, P. T. Chou, *Macromolecules* **2012**, *45*, 751–765.
7. Q. Wang, J. Ding, D. Ma, Y. Cheng, L. Wang, X. Jing, F. Wang, *Adv. Funct. Mater.* **2009**, *19*, 84–95.
8. Y. J. Pu, G. Nakata, F. Satoh, H. Sasabe, D. Yokoyama, J. Kido, *Adv. Mater.* **2012**, *24*, 1765–1770.
9. T. L. Chiu, P. Y. Lee, *Int. J. Mol. Sci.* **2012**, *13*, 7575–7585.
10. K. Udagawa, H. Sasabe, C. Cai, J. Kido, *Adv. Mater.* **2014**, *26*, 5062–5066.
11. J. J. Huang, M. K. Leung, T. L. Chiu, Y. T. Chuang, P. T. Chou, Y. H. Hung, *Org. Lett.* **2014**, *16*, 5398–5401.
12. M. Shakutsui, H. Matsuura, K. Fujita, *Org. Electron.* **2009**, *10*, 834–842.
13. S. R. Tseng, S. C. Lin, H. F. Meng, H. H. Liao, C. H. Yeh, H. C. Lai, S. F. Horng, C. S. Hsu, *Appl. Phys. Lett.* **2006**, *88*, 163501.
14. J. Chen, D. Ma, *Chem. Phys.* **2006**, *325*, 225–230.
15. S. K. Kim, C. J. Lee, I. N. Kang, J. H. Lee, J. W. Park, *Thin Solid Films* **2006**, *509*, 132–136.
16. T. Ye, M. Zhu, J. Chen, Q. Fu, F. Zhao, C. Shi, Y. Hu, D. Ma, C. Yang, *J. Mater. Chem.* **2012**, *22*, 6413–6418.
17. Y. Zhao, J. Chen, W. Chen, D. Ma, *J. Appl. Phys.* **2012**, *111*, 043716.
18. Y. Shirota, Y. Kuwabara, D. Okuda, R. Okuda, H. Ogawa, H. Inada, T. Wakimoto, H. Nakada, Y. Yonemoto, S. Kawami, K. Imai, *J. Lumin.*, **1997**, *72–4*, 985–991.
19. S. A. VanSlyke, C. H. Chen, C. W. Tang, *Appl. Phys. Lett.* **1996**, *69*, 2160–2162.
20. M. G. Helander, Z. B. Wang, J. Qiu, M. T. Greiner, D. P. Puzzo, Z. W. Liu, Z. H. Lu, *Science* **2011**, *332*, 944–947.
21. C. Xu, P. Cai, X. Zhang, Z. Zhang, X. Xue, J. Xiong, J. Zhang, *Sol. Energy Mater. Sol. Cells* **2017**, *159*, 136–142.
22. F. Wang, X. Qiao, T. Xiong, D. Ma, *Org. Electron.* **2008**, *9*, 985–993.
23. Z. Hongmei, X. Jianjian, Z. Wenjin, H. Wei, *Displays* **2014**, *35*, 171–175.
24. O. Hinsberg, *Ber.* **1886**, *19*, 483–488.
25. J. Harmenberg, B. Wahren, J. Bergman, S. Akerfeldt, L. Lundblad, *Antimicrob. Agents Chemother.* **1988**, *32*, 1720–1724.
26. J. Harmenberg, A. Akessonjohansson, A. Graslund, T. Malmfors, J. Bergman, B. Wahren, S. Akerfeldt, L. Lundblad, S. Cox, *Antivir. Res.* **1991**, *15*, 193–204.
27. K. Manna, Y. K. Agrawal, *Bioorg. Med. Chem. Lett.* **2009**, *19*, 2688–2692.
28. N. R. Pai, D. A. Pusalkar, *J. Chem. Pharm. Res.* **2010**, *2*, 485–493.
29. L. W. Deady, A. J. Kaye, G. J. Finlay, B. C. Baguley, W. A. Denny, *J. Med. Chem.* **1997**, *40*, 2040–2046.
30. C. H. Fan, P. P. Sun, T. H. Su, C. H. Cheng, *Adv. Mater.* **2011**, *23*, 2981–2985.
31. P. Tyagi, A. Venkateswararao, K. R. J. Thomas, *J. Org. Chem.* **2011**, *76*, 4571–4581.
32. K. R. J. Thomas, P. Tyagi, *J. Org. Chem.* **2010**, *75*, 8100–8111.
33. T. H. Su, C. H. Fan, Y. H. Ou-Yang, L. C. Hsu, C. H. Cheng, *J. Mater. Chem. C* **2013**, *1*, 5084–5092.
34. A. Venkateswararao, P. Tyagi, K. R. J. Thomas, P. W. Chen, K. C. Ho, *Tetrahedron* **2014**, *70*, 6318–6327.
35. X. Qian, H. H. Gao, Y. Z. Zhu, L. Lu, J. Y. Zheng, *J. Power Sources* **2015**, *280*, 573–580.
36. E. Schunk, L. Marchlewski, *Ber.* **1895**, *28*, 2525–2531.
37. A. V. Ivashchenko, V. M. Dziomko, *Russ. Chem. Rev.* **1977**, *46*, 115–120.
38. R. Dowlatabadi, A. Khalaj, S. Rahimian, M. Montazeri, M. Amini, A. Shahverdi, E. Mahjub, *Synth. Commun.* **2011**, *41*, 1650–1658.
39. A. J. Payne, J. S. J. McCahill, G. C. Welch, *Dyes And Pigments* **2015**, *123*, 139–146.
40. J. R. Pouliot, F. Grenier, J. T. Blaskovits, S. Beaupre, M. Leclerc, *Chem. Rev.* **2016**, *116*, 14225–14274.
41. M. L. Sun, W. S. Zhu, Z. S. Zhang, C. J. Ou, L. H. Xie, Y. Yang, Y. Qian, Y. Zhao, W. Huang, *J. Mater. Chem. C* **2015**, *3*, 94–99.
42. C. Tang, R. Bi, Y. Tao, F. Wang, X. Cao, S. Wang, T. Jiang, C. Zhong, H. Zhang, W. Huang, *Chem. Commun.* **2015**, *51*, 1650–1653.
43. W. Lu, J. Kuwabara, T. Kanbara, *Macromolecules* **2011**, *44*, 1252–1255.
44. M. Wakioka, Y. Kitano, F. Ozawa, *Macromolecules* **2013**, *46*, 370–374.
45. Q. H. Feng, Y. I. Han, M. N. Yu, B. Li, Y. Wei, L. H. Xie, W. Huang, *Chin. J. Polym. Sci.* **2017**, *35*, 87–97.
46. L. Wang, G. W. Zhang, C. J. Ou, L. H. Xie, J. Y. Lin, Y. Y. Liu, W. Huang, *Org. Lett.* **2014**, *16*, 1748–1751.
47. J. F. Zhao, J. I. Wong, J. K. Gao, G. Li, G. C. Xing, H. C. Zhang, T. C. Sum, H. Y. Yang, Y. L. Zhao, S. L. A. Kjelleberg, W. Huang, S. C. J. Loo, Q. C. Zhang, *RSC Adv.* **2014**, *4*, 17822–17831.
48. J. B. Li, Q. C. Zhang, *ACS Appl. Mater. Inter.* **2015**, *7*, 28049–28062.
49. J. B. Li, S. Chen, Z. L. Wang, Q. C. Zhang, *Chem. Rec.* **2016**, *16*, 1518–1530.
50. G. Li, H. M. Duong, Z. Zhang, J. Xiao, L. Liu, Y. Zhao, H. Zhang, F. Huo, S. Li, J. Ma, F. Wudl, Q. Zhang, *Chem. Commun.* **2012**, *48*, 5974–5976.
51. H. M. Zhang, Q. Fu, W. J. Zeng, D. G. Ma, *J. Mater. Chem. C* **2014**, *2*, 9620–9624.
52. C. T. Lee, W. T. Yang, R. G. Parr, *Phys. Rev. B* **1988**, *37*, 785–789.
53. G. W. T. M. J. Frisch, H. B. Schlegel, G. E. Scuseria, M. A. Robb, J. R. Cheeseman, G. Scalmani, V. Barone, B. Mennucci, G. A. Petersson, H. Nakatsuji, M. Caricato, X. Li, H. P. Hratchian, A. F. Izmaylov, J. Bloino, G. Zheng, J. L. Sonnenberg, M. Hada, M. Ehara, K. Toyota, R. Fukuda, J. Hasegawa, M. Ishida, T. Nakajima, Y. Honda, O. Kitao, H. Nakai, T. Vreven, J. A. Montgomery, Jr., J. E. Peralta, F. Ogliaro, M. Bearpark, J. J. Heyd, E. Brothers, K. N. Kudin, V. N. Staroverov, R. Kobayashi, J. Normand, K. Raghavachari, A. Rendell, J. C. Burant, S. S. Iyengar, J. Tomasi, M. Cossi, N. Rega, J. M. Millam, M. Klene, J. E. Knox, J. B. Cross, V. Bakken, C. Adamo, J. Jaramillo, R. Gomperts, R. E. Stratmann, O. Yazyev, A. J. Austin, R. Cammi, C. Pomelli, J. W. Ochterski, R. L. Martin, K. Morokuma, V. G. Zakrzewski, G. A. Voth, P. Salvador, J. J. Dannenberg, S. Dapprich, A. D. Daniels, O. Farkas, J. B. Foresman, J. V. Ortiz, J. Cioslowski and D. J. Fox, *Gaussian 09, Revision B.1*, Gaussian, Inc., Wallingford CT, **2009**.
54. J. Zhao, J. I. Wong, C. Wang, J. Gao, V. Z. Y. Ng, H. Y. Yang, S. C. J. Loo, Q. Zhang, *Chem. Asian J.* **2013**, *8*, 665–669.

FULL PAPER

Direct arylation: Symmetrical 6*H*-indolo[2,3-*b*]quinoxaline derivative implanted with tetrafluoro-*p*-phenylene plays as an effective hole injection layer material in organic light emitting devices.



Dai Dong, Da Fang, Hairong Li,
Caixia Zhu, Xianghua Zhao,
Jiewei Li, Lingzhi Jin, Linghai
Xie, Lin Chen, Jianfeng Zhao,*
Hongmei Zhang,* Wei Huang*

Page No. – Page No.

C-H Direct Arylated 6*H*-
Indolo[2,3-*b*]quinoxaline
Derivative as Thickness-
Dependent Hole Injection Layer

Supporting Information for**C-H Direct Arylated 6H-Indolo[2,3-b]quinoxaline Derivative as Thickness-Dependent Hole Injection Layer**

Dai Dong,^a Da Fang,^b Hairong Li,^a Caixia Zhu,^a Xianghua Zhao,^c Jiewei Li,^a Lingzhi Jin,^b Linghai Xie,^b Lin Chen,^d Jianfeng Zhao,^{*a,b} Hongmei Zhang,^{*b} Wei Huang^{*a,b}

^aKey Laboratory of Flexible Electronics (KLOFE) & Institute of Advanced Materials (IAM), Jiangsu National Synergetic Innovation Center for Advanced Materials (SICAM), Nanjing Tech University (NanjingTech), 30 South Puzhu Road, Nanjing 211816, P.R. China

^bKey Laboratory for Organic Electronics & Information Displays (KLOEID) and Institute of Advanced Materials, Nanjing University of Posts & Telecommunications, Nanjing 210023, P.R. China

^cCollege of Chemistry and Chemical Engineering, Xinyang Normal University, Xinyang 464000, Henan, China

^dNanjing Polytechnic Institute, Nanjing 210048, P.R. China

Contents:

Figure S1. GC-MS of 9-BrC₈IQ

Figure S2. ¹H NMR of 9-BrC₈IQ

Figure S3. MALDI-TOF MS of TFBIQ

Figure S4. ¹H NMR of TFBIQ

Figure S5. TGA curve of TFBIQ

Figure S6. DSC curve of TFBIQ

Table S1. Theoretical calculation of TFBIQ vs non-fluorinated BIQ

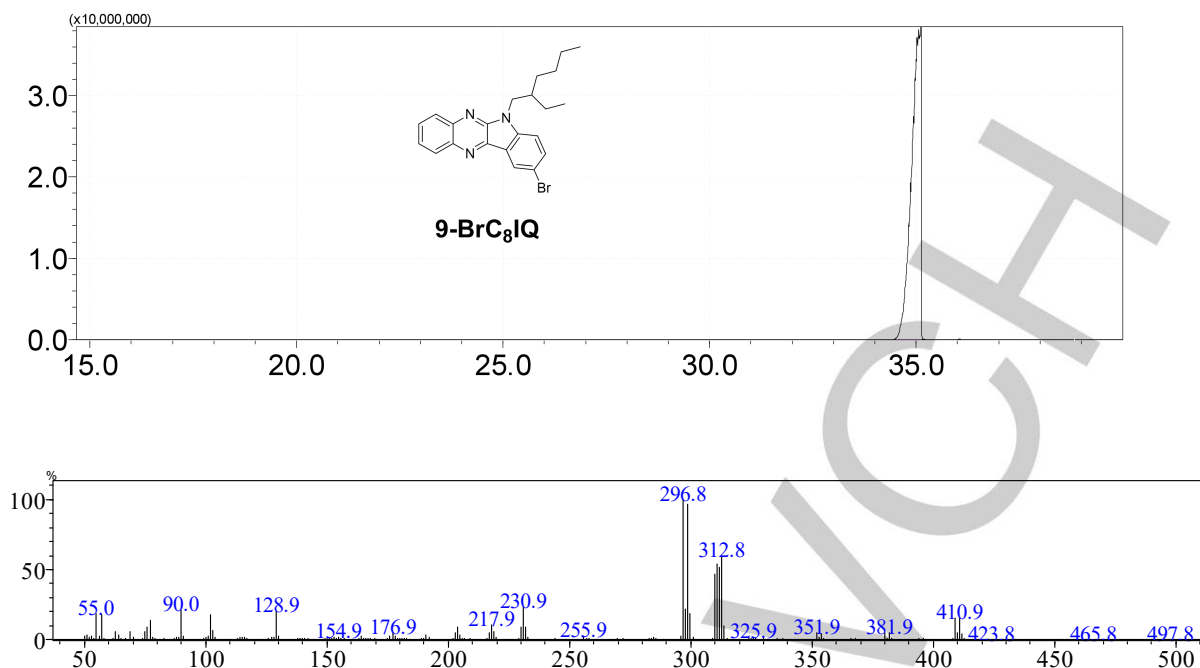


Figure S1. GC-MS of 9-BrC₈IQ

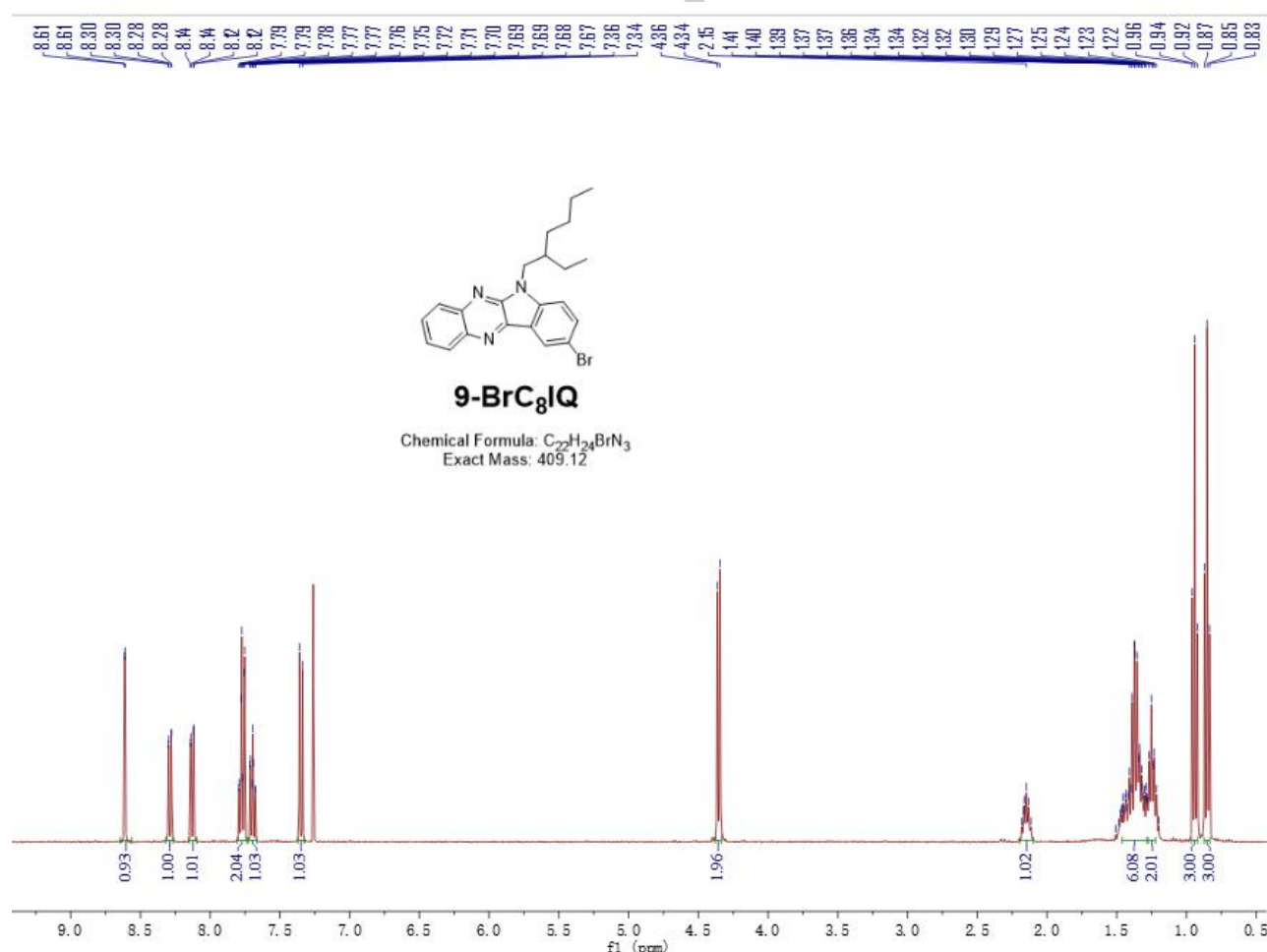


Figure S2. ¹H NMR of 9-BrC₈IQ

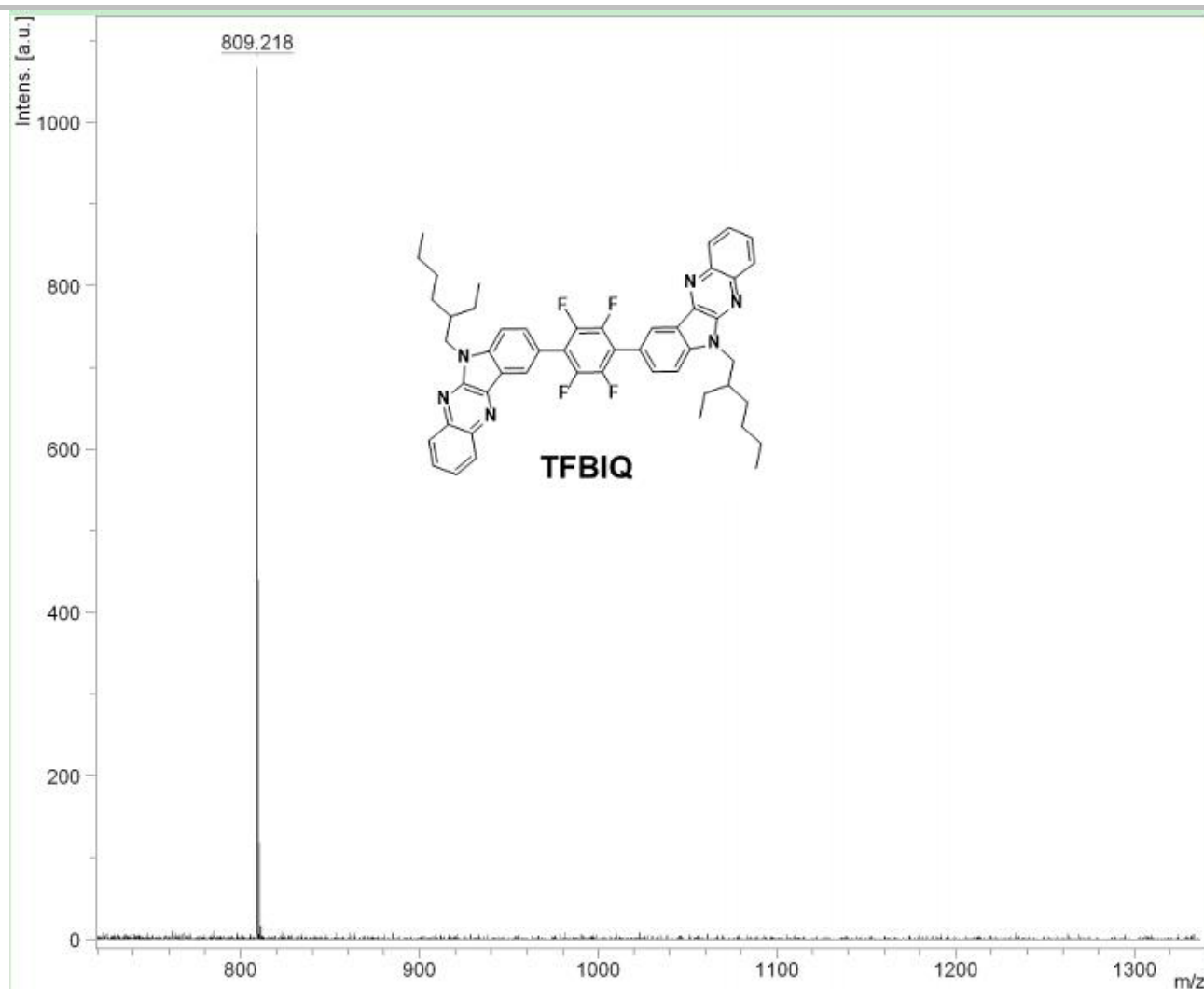


Figure S3. MALDI-TOF MS of TFBIQ

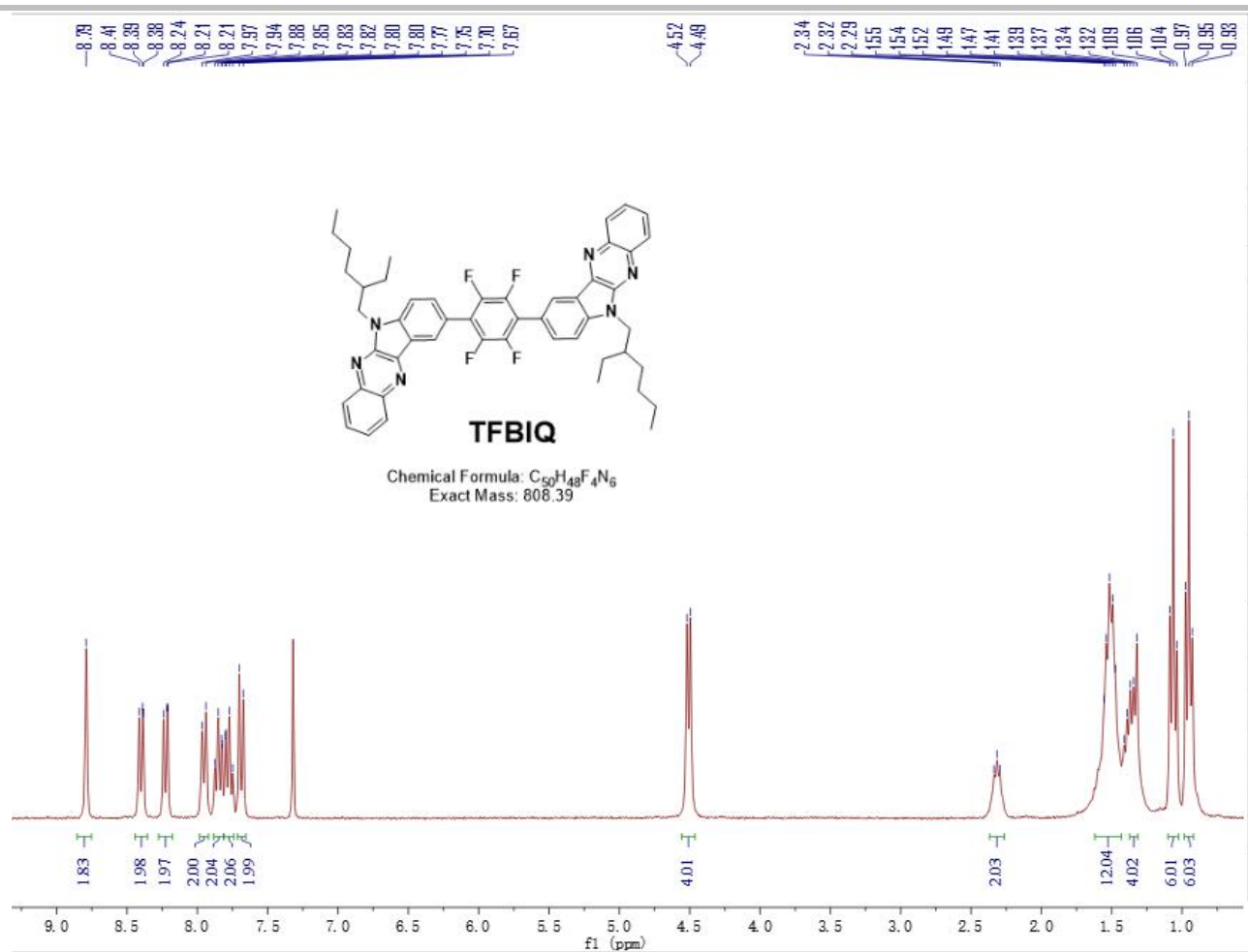


Figure S4. ¹H NMR of TFB IQ

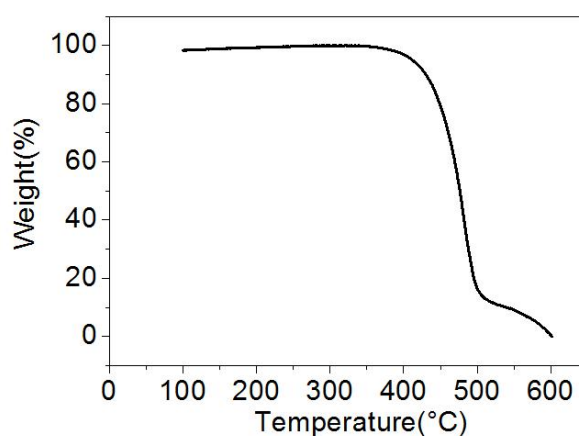


Figure S5. TGA curve of TFB IQ

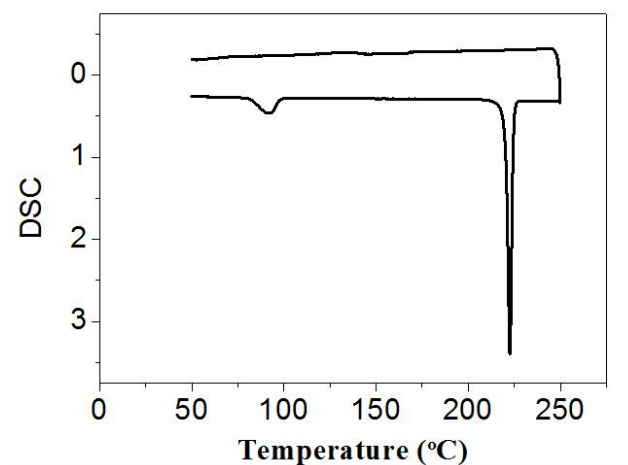




Figure S6. DSC curve of **TFBIQ**

Table S1. Theoretical calculation of the symmetrical tetrafluorinated **TFBIQ** vs non fluorinated one.

Energy level	 TFBIQ	 BIQ
Ground	-2111.12214103	-1714.31059972
Ground+	-2110.85099264	-1714.05179844
cation	-2110.85934041	-1714.06233165
Cation0	-2111.11223742	-1714.30033133
IP _v	-7.378327299646 (eV)	-7.042345150592
IP		
Hole Reorganization energy	0.496645601732 (eV)	0.56604065824
Method	wb97xd/6-31g(d)	wb97xd/6-31g(d)